TITLE: **FIR laser beam & Telescope Simulator: test report**

By: Marc Ferlet (RAL)

DISTRIBUTION

- RAL/SSTD - SPIRE Project Team:
  For info:
  - B Swinyard (RAL)
  - D Smith (RAL)
  - T Lim (RAL)
  - E Sawyer (RAL)

  For Project database/archive:
  - J Long (RAL)

- University of Lethbridge – SPIRE Test Team:
  - S Ronayette (UoL)

CHANGE RECORD

ISSUE	DATE	SECTION	REASON FOR CHANGE
1.0	04/05/04	All	First issue of the document
1.1	10/05/04	5 & Annex	Update of results

CONTENTS

APPLICABLE AND REFERENCE DOCUMENTS

RD1 SPIRE-RAL-NOT-000621v4
RD2 SPIRE-RAL-NOT-000622v3
RD3 SPIRE RAL-NOT-000734v2
RD4 SPIRE-RAL-NOT-001258v1
RD5 SPIRE calibration lab / Laser log-book

1. Introduction

This note summarises a series of experiments performed with the FIR laser in the SPIRE calibration lab over the last few months. Although several notes have been circulated around within the Project and have been already included in log book, it was found useful to compile in a single TN the results of these tests concerning one of the SPIRE ground-calibration source and related instrumentation.
An illustrated view of the lab set-up is given in section 2. Results of FIR beam alone (i.e. limited propagation within the system) characterisation from measurements made at ~214μm are reported in section 3. Section 4 & 5 deal with laser beam profiles at the image planes (best focus) of Telescope Simulator in reduced and full (i.e. including path through image space scan system, cryostat FIR window and cryostat filters) respectively.

2. Brief description of the optical systems

The optical instrumentation used in the different test is illustrated in the pictures below. The 2 pictures focus on the present instrumentation on the 2 main optical benches outside the cryostat. Details of the design and implementation, component and system particularly for the Telescope Simulator, are given in RD1-4.
Only section 4 & 5 are using partially or completely the instrumentation shown below. Simplified test configuration for FIR laser only characterisation is described along side the results in section 3.

Although the optical systems on the separate benches are protected by enclosures which can be purged with dry air to limit the effect of atmospheric absorption over a max optical path (outside cryostat) estimated to ~6m, none of the tests in the following section used the purge system (i.e. propagation in air).

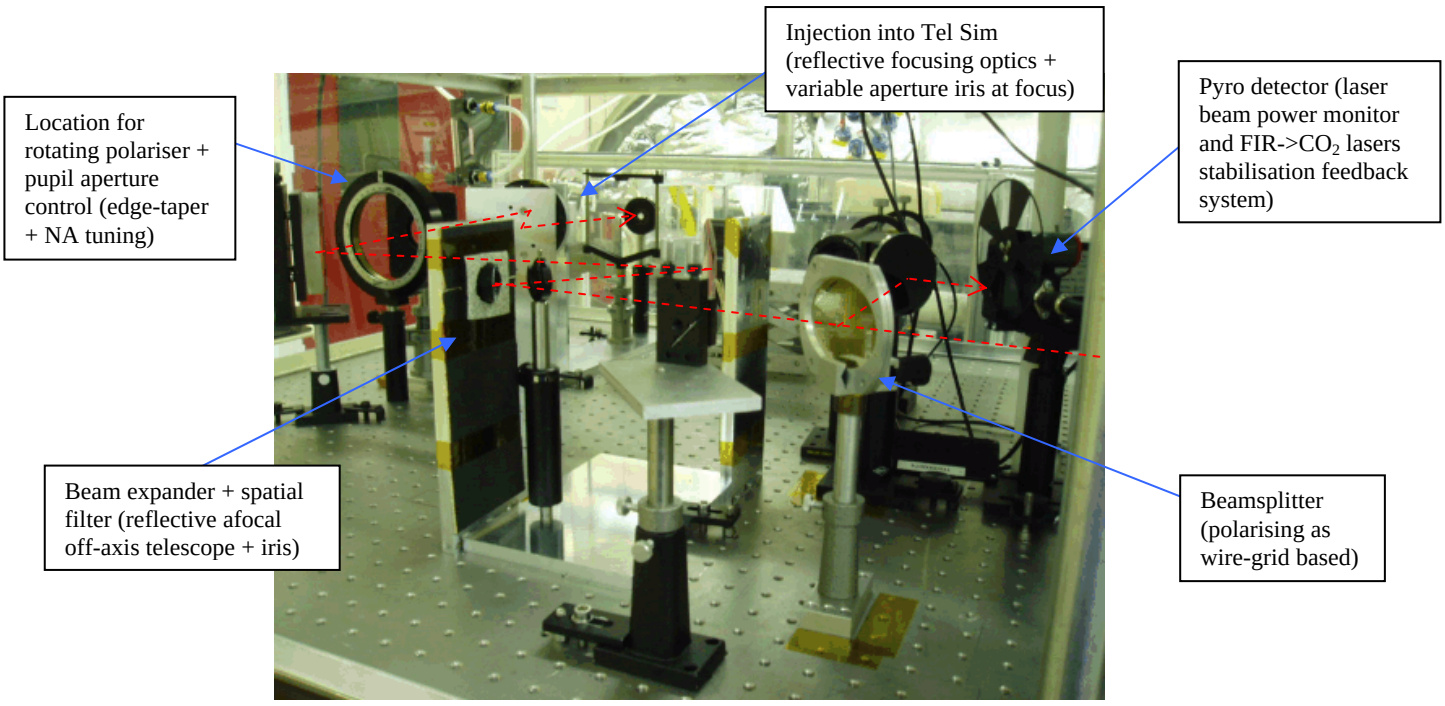

Figure 1: FIR laser bench set-up (05/05/2004). The FIR laser beam path from the FIR cavity output window (+ 100cm^{-1} long pass edge filter) is outlines in red (dashed line). Extra alignment components such as HeNe laser + beam expander + mirror are also present.

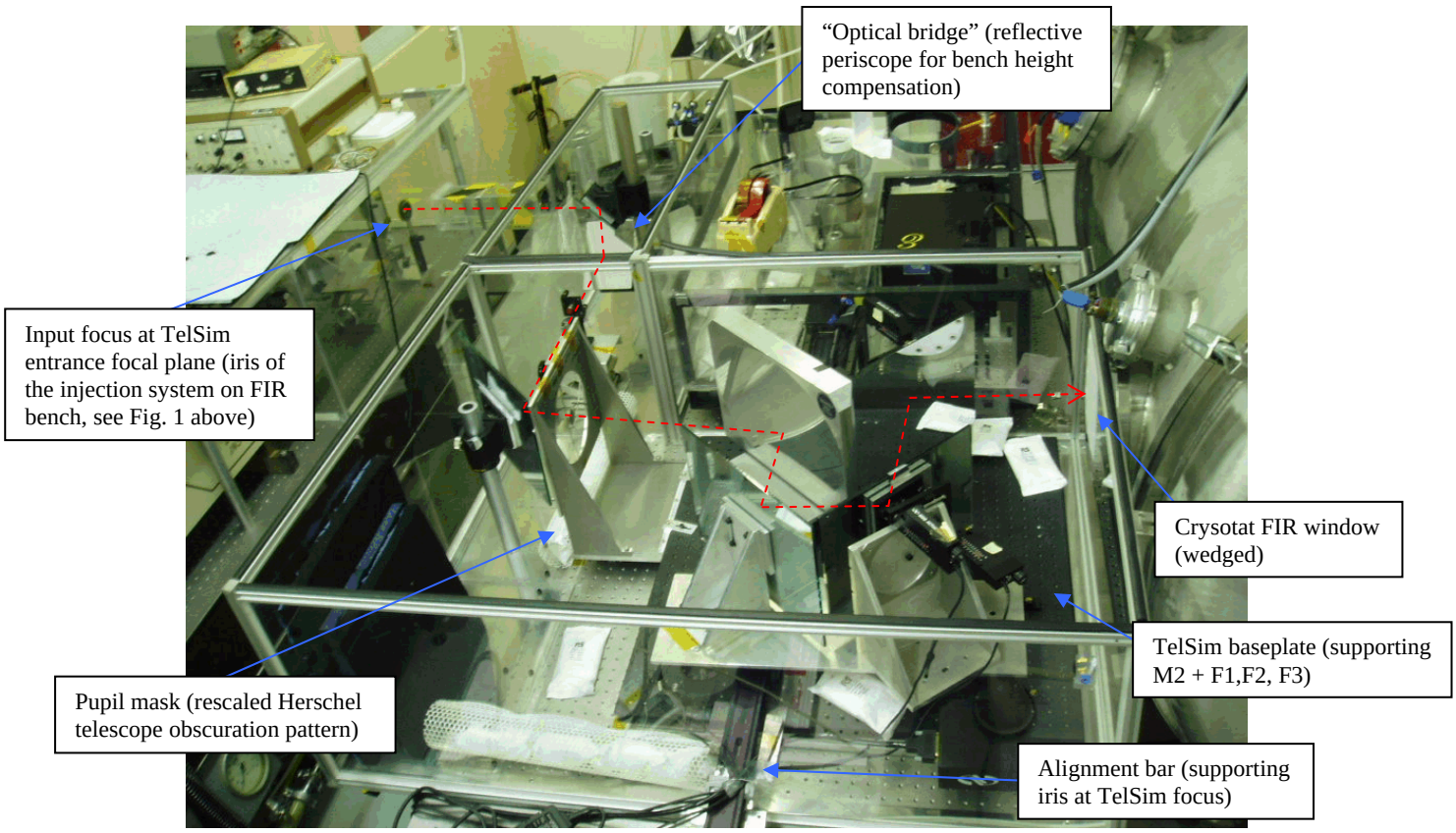

Figure 2: Telescope Simulator main bench (05/05/2004). The FIR laser beam path from the FIR bench output to the calibration cryostat optical port (FIR window) is outlines in red (dashed line).

3. FIR laser beam test & characterisation

Report on the FIR laser beam characterisation. Test performed in SPIRE cryolab on 30/09/03.

FIR output wavelength: 214μm, linear vertical polarisation (verified with rotated wire grid)

FIR beam total power: ~2mW max at cavity output

Optics: Off-axis (60°) single paraboloid, Al protected (Janos Tech), f_{eff}=152.4mm, located ~900mm from laser cavity output plane

Detector (at optics focus): Spiricon/PYROCAM III, room-temperature pyroelectric 124x124 detector array, pixel size~100μm (demo. on-site by UK distributor Elliot Scientific)

Remarks: FIR beam considered as stable enough, no use of the stabilisation feedback system; manual alignment of camera wrt beam focus.

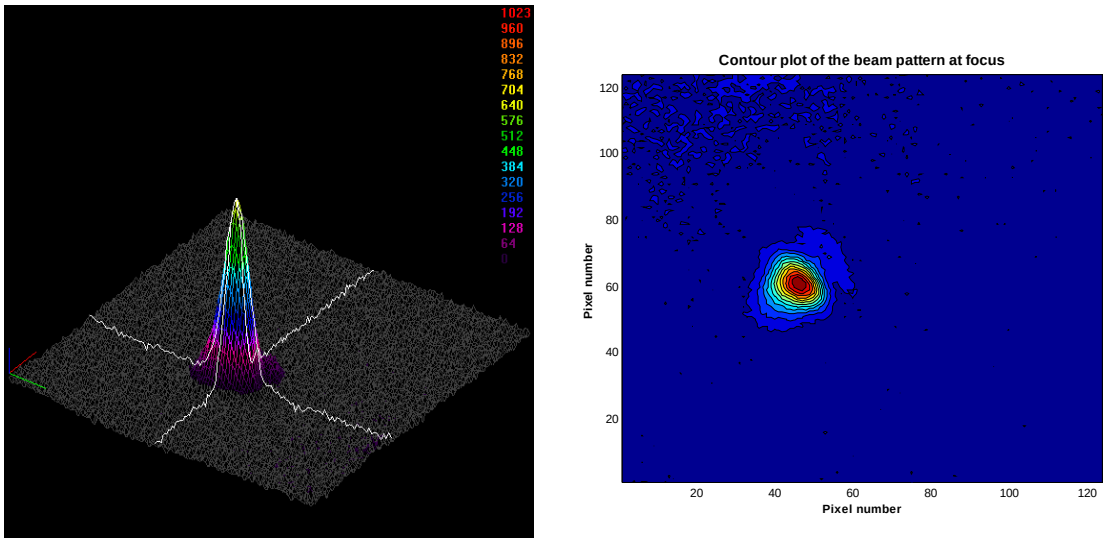

Figure 3: Beam pattern (3D intensity view and contour plot) of the focused FIR laser beam at 214µm after acquisition by PYROCAM III camera system. Summation and averaging were used to improve SNR.

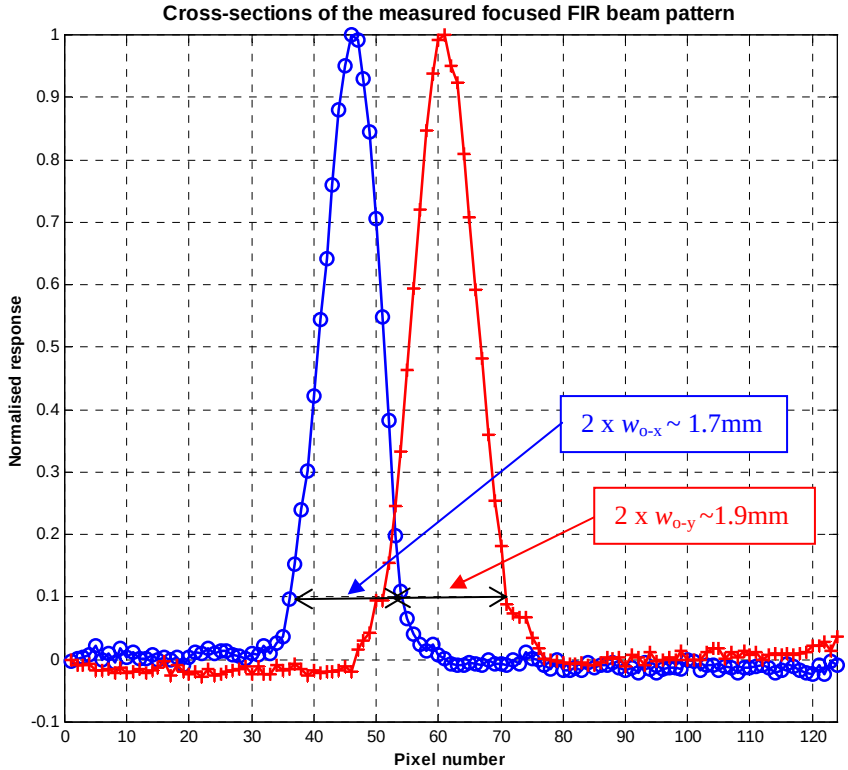

The above values for the waist were obtained by fitting a FMGB to the normalised data for the 2 main planes (see below). The average value for the waist is w_o=0.9±0.1mm when a FMGB is assumed. The ~10-15% uncertainty arises from the sampling at detector as well as some potential residual astigmatism and coma from angular misalignment in (manual) camera positioning.

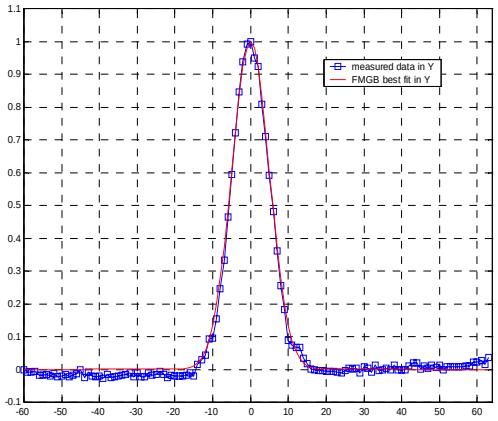

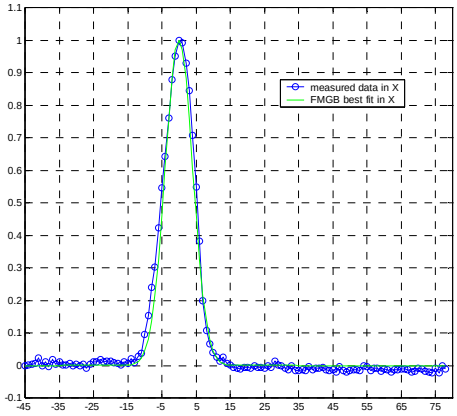

Under the same assumption that the FIR cavity is delivering a FMGB, we can in parallel estimate the expected wait size at mirror focus. The test configuration (different from figure 2) is summarised by the sketch below.

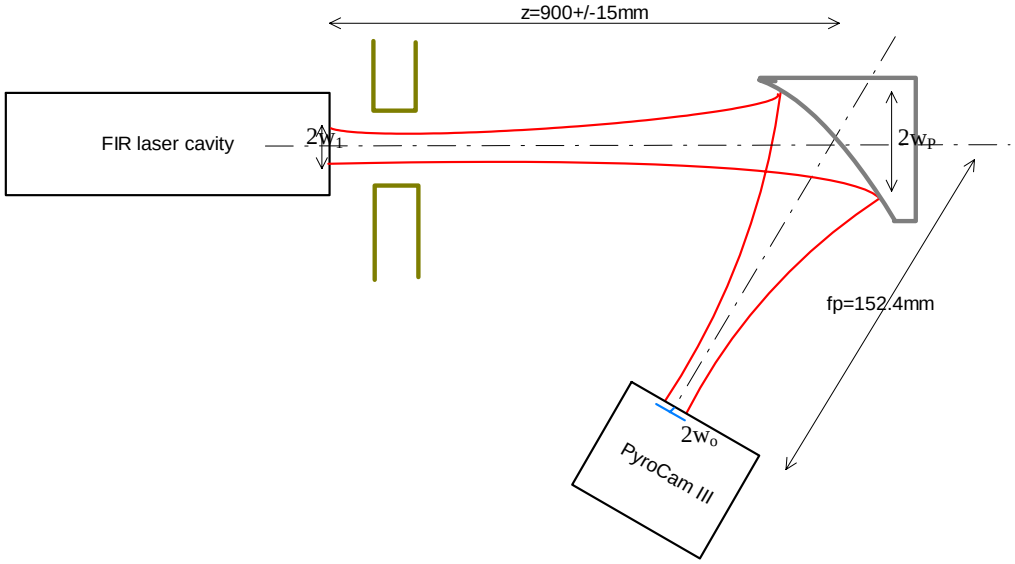

The laser starts with an initial waist w_1=6.0±0.5mm at the output of the FIR cavity. The free-space propagation of the assumed single mode GB up to the paraboloid mirror gives rise to a $1/e^2$ beam radius w_p on the mirror given by:

$$> \quad wp := w1\sqrt{1+\left(\frac{\lambda\, z}{\pi\, w1^2}\right)^2}$$

Its value is w_p=11.85mm at λ=214μm. We can check at this point that the mirror is well oversized (aperture diameter is 76.2mm) compared to the beam so that no noticeable additive diffraction effect from (low) illuminated mirror edge is to be expected here. The parabolic mirror refocuses the beam and the new waist w_o assumed to be located close to geometric focus (not probed in the experiment) and where the camera is located is given by:

$$> \quad wo := \frac{fp\,\lambda}{\pi\, wp}$$

One can also consider the angular aperture approach which gives $w_o=(2/\pi)F\lambda$ where the focal ratio for $1/e^2$ is given by $F=f_p/(2w_p)$. As F~6.4 here, the focused beam is slow enough for the paraxial approximation to apply and both formulas lead to w_o=0.88mm.
Uncertainty on this value results from the addition (error assumed independent) of the ~2% relative uncertainty on the distance z and the ~8% uncertainty on the initial waist size w_1. The final theoretical estimation of the expected waist size for a FMGB FIR line in this configuration is w_o=0.88mm±10%. This agrees well with the above measurement and allows concluding that, at first order (under FMGB approximation) the FIR laser line at 214µm delivers a coherent single mode Gaussian beam.

4. Laser beam measurement at TelSim focus

Test performed in SPIRE cryolab on 16/12/03 with Golay cell (+ chopper) at the TelSim focus located at the end of the alignment bar (see Fig 2; F1 removed, direct path from M2 to detector at focus). Details of the FIR laser status and experimental conditions are given in RD5.

NB: The experiment was carried out after the replacement of the FIR laser Brewster window (ZnSe plate) at the entrance of the FIR laser cavity.

Beam size only measurements performed at 2 different wavelengths:

- 214µm (FIR gas = DFM) for comparison with above (section 3) measurements,
- 392µm (FIR gas = MA) for longer wavelength effect assessment (e.g. increase in diffraction).

Modelling of the expected beam pattern and comparison with experimentally measured beam size along vertical axis is given below.

Convolution of Gaussian function => application to finite aperture detector effect (e.g. the Golay cell entrance aperture) on single mode Gaussian Beam detection.

```
> restart;func_f:=x->exp(-x^2/wo^2);
```

$$func\_f := x \rightarrow \mathbf{e}^{\left(-\frac{x^2}{wo^2}\right)}$$

```
> convol:=int(func_f(x-t),t=(-L/2)..(L/2));
```

$$convol := \frac{1}{2}\sqrt{\pi}\ wo\ \mathrm{erf}\left(\frac{L-2x}{2\ wo}\right)+\frac{1}{2}\sqrt{\pi}\ wo\ \mathrm{erf}\left(\frac{L+2x}{2\ wo}\right)$$

At TelSim input focus (FIR bench: output of the injection system, see Fig 1) at 214µm:

```
>L:=3;lambda:=0.214;F_number:=8;wo:=evalf((2/Pi)*F_number*lambda);plo
t(convol/maximize(convol,x=-5..5),x=-4..4);
```

$$L := 3$$

$$\lambda := 0.214$$

$$F\_number := 8$$

$$wo := 1.089893050$$

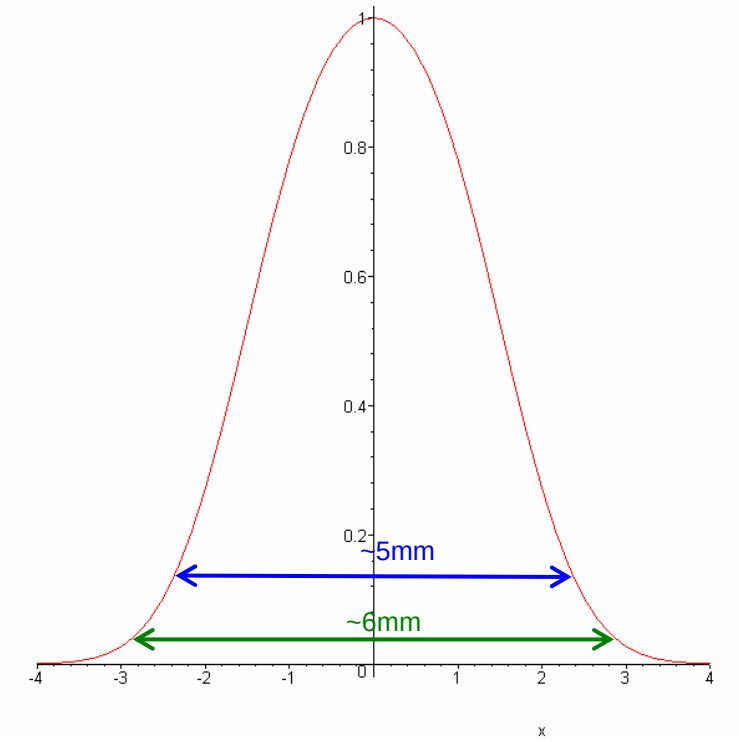

The blue arrow range is the estimate of the $1/e^2$ beam diameter from measurement and the green arrow range is the estimated full beam diameter from measurement at the limit of detection (limited by background noise + detector noise, absorption through long path) with the Golay cell. Agreement with the model is good although more flat-top central shape is expected (difficult to characterize due to measurement uncertainty linked to laser output stability).

At TelSim final focus (see Fig. 2; F1 removed), same detector (Golay cell), at 392µm:

```
>L:=3;lambda:=0.392;F_number:=8.7;wo:=evalf((2/Pi)*F_number*lambda);plot(convol/maximize(convol,x=-5..5),x=-6..6);
```

$$L := 3$$

$$\lambda := 0.392$$

$$F\_number := 8.7$$

$$wo := 2.171128071$$

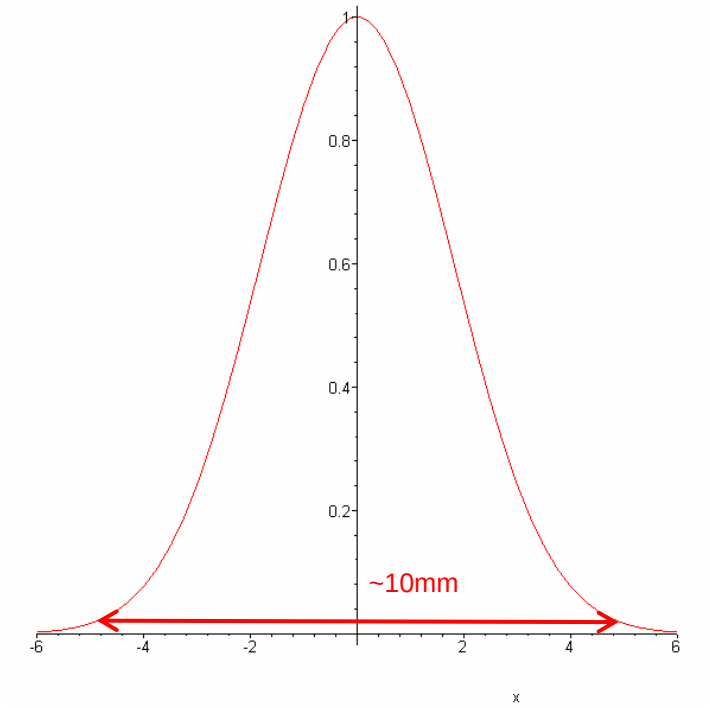

Full beam diameter estimate by measurement is show in red arrow range. The level of detection may be higher than shown above but the edge-taper at pupil mask will increase by 5-10% the waist at focus so the agreement appears good also at long wavelength.

NB: fluctuations of 15-20% minimum in average on the measured signal were recorded during the tests.

5. Laser beam measurement at TelSim focus inside Calibration cryostat

This series of tests was performed on 22 and 23/04/04 and used the complete path, as described in section 2, from FIR laser cavity to focal plane inside calibration cryostat (ultimately confocal with the entrance focal plane of SPIRE during ground-testing).
The tests were performed after the 1st series of SPIRE CQM performance tests. Some of these tests used the FIR laser at 432μm (FIR gas =FA; see RD5) i.e. the centre of SPIRE PLW band. The full PLW focal plane array response to point source illumination with the laser was not expected. Although laser illumination of the array might have been far above the detection range of SPIRE, it was found necessary to assess if the point source laser illumination issue is not coming from instrumental effect outside SPIRE itself (i.e. bulk and/or surface scattering from cryostat window, speckle from coherence effect after multiple reflections within tilted cryostat filter, …). The results discussed in section 4 demonstrates that the TelSim is focussing well the injected laser beam into a GB pattern focal plane irradiance in good agreement with expected diffraction-limited beam shape from theory.

The specific detection system located temporary inside the cryostat is shown in the picture below.

Attenuation of the beam was found to be needed and performed via insertion of paper in the collimated section of the beam path on the FIR bench. Calibration of the paper showed an attenuation of ~1.05±0.10dB/sheet, very reproducible and consistent with same data obtained during SPIRE CQM test campaign at he same wavelength.

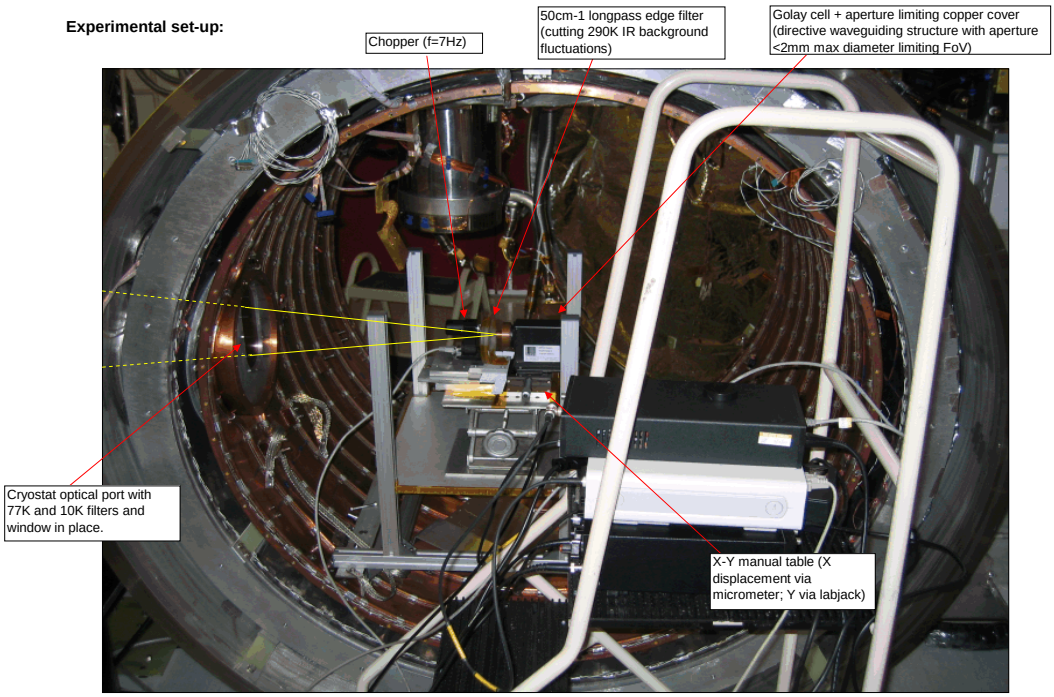

Figure 4: Details of the experimental detection system used for laser beam profile measurement inside cryostat.

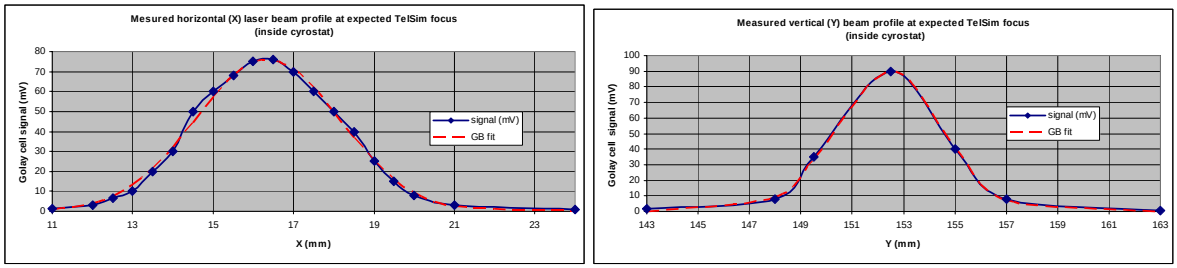

Figure 5: Measured (and fits) transverse laser beam profiles at best focus inside cryostat

Using the TelSim multi-axes control, defocus was induced via displacement of the Trombone formed by the combination of F1+F2. Then 2 other transverse profiles were manually recorded. The laser output was found very stable during the each data recording period.

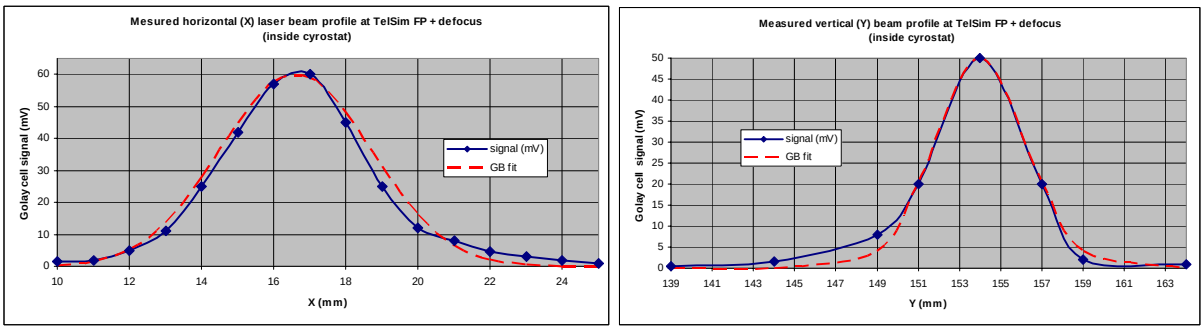

Figure 6: idem at figure 5 but with 30mm defocus on TelSim.

NB: The laser output showed fluctuations of ~5% in the best focus case and ~11% in magnitude during the defocus beam probing.

From the fitted (GB spatial model) experimental data, the following measured beam characteristic parameters (waist size at best focus and beam radius at defocus position) at 432µm were derived:

F= 8.68 **wo theo= 2.48** **for ~4.5 dB edge taper**

Best fits in x:	**wo x (mm)**	**FWHMo x (arcsec)**	**wz x (mm)**	**FWHMz x (arcsec)**
	2.52	**30.42**	**2.95**	**35.58**
Best fits in y:	**wo y (mm)**	**FWHMo y (arcsec)**	**wz y (mm)**	**FWHMz y (arcsec)**
	2.91	**35.03**	**3.17**	**38.15**
Averages=	**2.72**	**32.72**	**3.06**	**36.86**

The (Herschel-)equivalent FWHM on sky are given as indications. Applying FMGB propagation law, the defocus value in x and y are well-explained for a 30mm defocus from best focal plane (but it is not clear that the TelSim was providing a ~30mm defocus from GO focal plane). Difference in beam size in x and y may come from the relative lack of precision on the y measurement (labjack vertical displacement compared to micrometer control in x). Residual TelSim astigmatism along side beam polarisation could also contribute (TBI) to the slight elliptical shape, elongated along y (i.e. the SPIRE Phot long length direction).

It was also checked that for the above derived parameters (see attached spreadsheet "***SPIRE_FIRlaser+TelSim characterisation.xls***"), the closest GSM (=Gaussian Shell Model) is well within the paraxial approximation of the spatial-spectral domain.

- Through-focus:

By varying the TelSim trombone position, a through-focus probing of the peak beam irradiance at different out-of-focus plane was performed. For each defocus, position compensation with TelSim scan angular control (2-axes, on F2 and F3) was made.

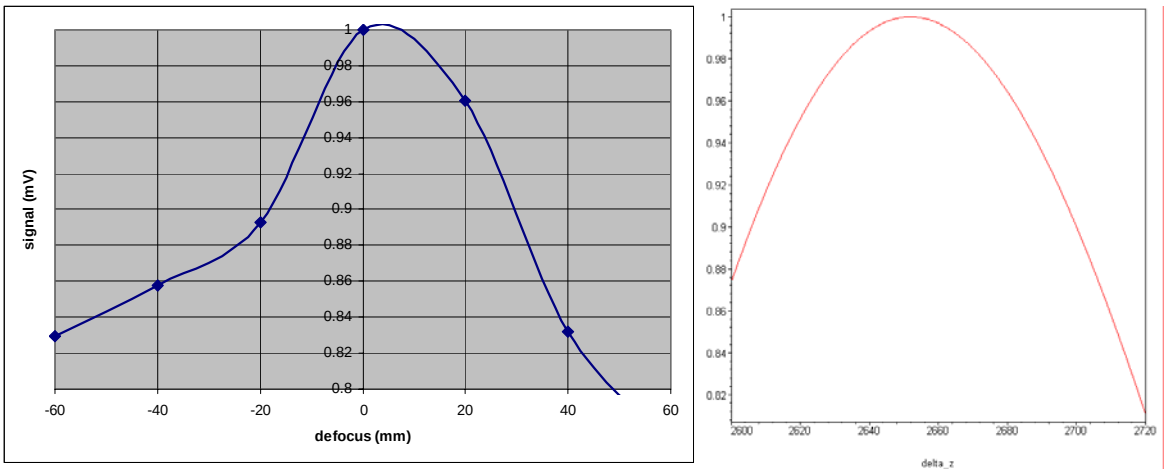

Figure 7: Normalised beam peak irradiance: as-measured (left) and as-modelled (right).

The measurements are compared to simulation from a model based on diffracted truncated GB with an axial irradiance given (before normalisation) by the following closed-form expression:

$$Iaxial := z \rightarrow \frac{2\,\pi\,a^2\,T^2\left(\coth\left(\frac{1}{T^2}\right)-\frac{\cos\left(\frac{\pi\,N\,(R-z)}{z}\right)}{\sinh\left(\frac{1}{T^2}\right)}\right)}{\lambda^2\,z^2\left(1+\frac{\pi^2\,T^4\,N^2\,(R-z)^2}{z^2}\right)}$$

where a is the radius of the Herschel exit pupil (virtual simulated), T is the truncation parameter set to represent the estimated ~4.5dB edge-taper from the experiment, R is the distance from simulated exit pupil to best geometric focus and N is the Fresnel number (here ~20). From Figure 7 above, one can see that qualitative agreement is found, although deeper interpretation would be difficult due to estimated ~20% relative uncertainty on the measurements (laser fluctuations + reset during the measurement campaign; angular misalignment of the detector with fixed pointing during through-focus scan wrt to TelSim beam). Nevertheless the axial region over which the Strehl ratio is > 85% is in agreement with the depth of focus (approx. the Rayleigh range).

- Modal decomposition:

Based on the assumption that the detected beam could be a general partially coherent beam of GSM type formed by independent superposition of Hermite-Gauss modes, a modal structure decomposition, see below, has been performed on the fitted data (averaged value at best focus):

$$I_{fitted\ data}(x)=\sum_{n=0}^{\infty}c_n.\left(HG_n(x)\right)^2 \quad \text{with} \quad HG_n(x)=\left(\frac{2}{\pi\,\omega_o}\right)^{1/4}.\frac{1}{\sqrt{2^n\,n!}}.H_n\left(\frac{x\sqrt{2}}{\omega_o}\right).e^{-\frac{x^2}{\omega_o^2}}$$

$$\text{and} \quad c_n=2\pi^2\,\omega_o^2\int_0^{\infty}FT\left[I_{fitted\ data}(x)\right](u).\Psi_n(\pi^2\,\omega_o^2\,u^2).u.du \quad \text{with} \quad \Psi_n(t)=L_n(t).e^{-t/2}$$

where H_n and L_n are the n^{th}-order Hermite and Laguerre polynomials respectively. One can see from the graph below that the delivered beam is single-moded at ~91%. The apparition of less than 10% of higher order mode (1 and 2) can be understood as resulting from diffraction and scattering at the different optical components and apertures through the complete path. This relatively low content of higher mode indicates a good and "clean" propagation through the system.

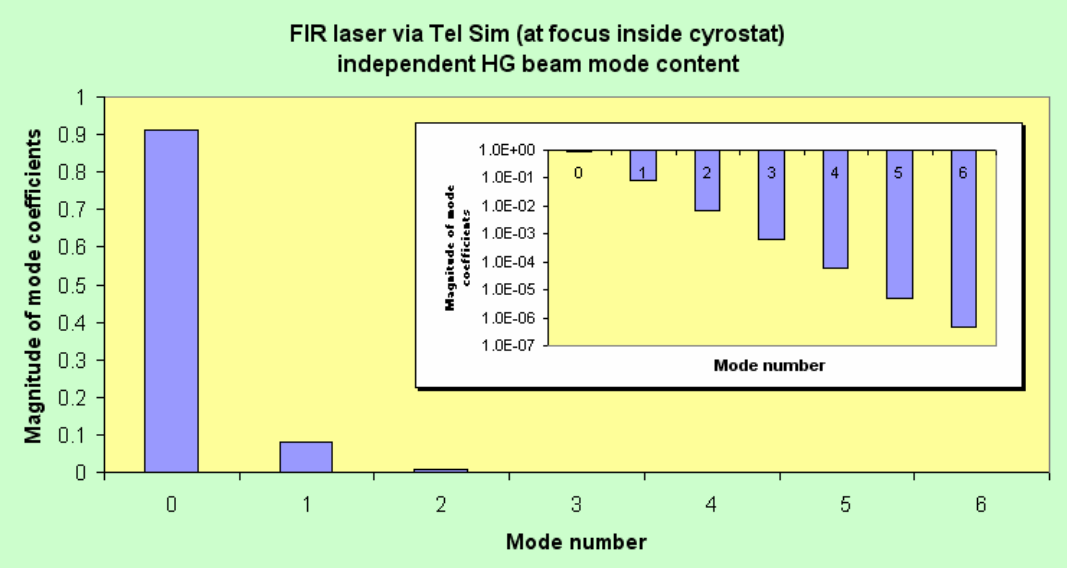

Error in the mode coefficient increases exponentially: assuming ~5% on C_0, it becomes ~51% on C_1, ~107% on C_2 and so on… But the insert in the above figure shows the rapid (actually exponential) decreases of the mode coefficients so that large errors on higher order have no impact on the main interpretation. The M^2 factor was estimated very close to ~1.1-1.2.

Annex

Experimental set-up and location of best focus:

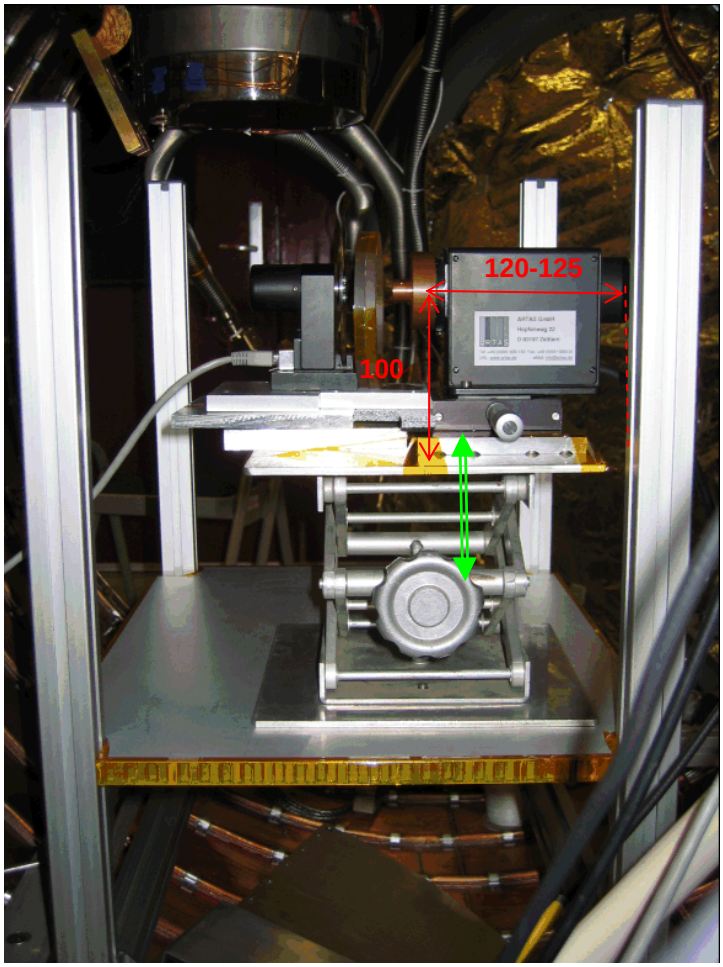

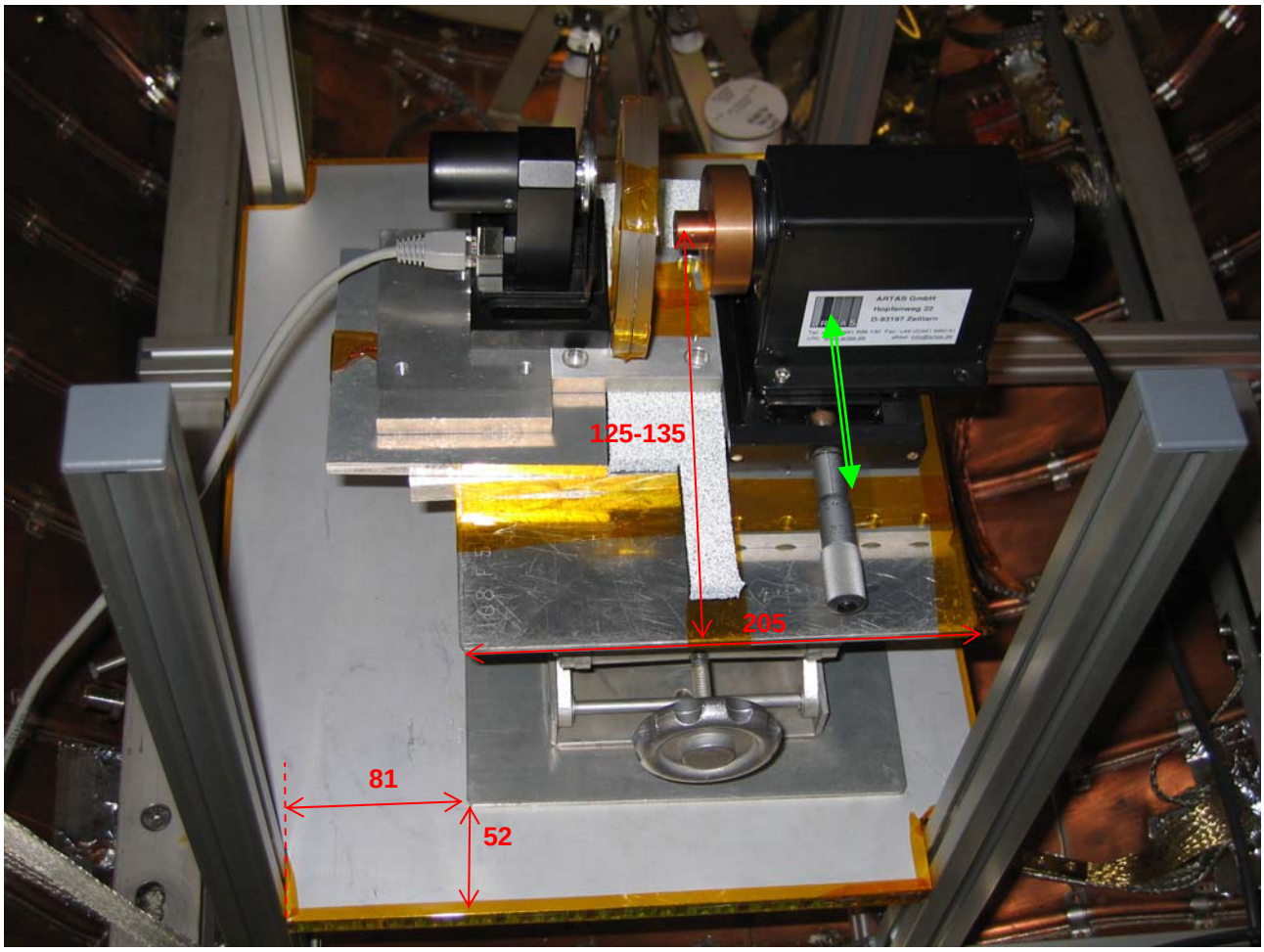
125-135
205
81
52